JOURNAL OF MATERIALS SCIENCE 37 (2002) 4581–4587

Effect of Co substitution for Mn on $Y_{1-x}Sr_xMnO_3$ properties for SOFC cathode material

CHING-YING HUANG, TA-JEN HUANG*
Department of Chemical Engineering, National Tsing Hua University, Hsinchu, Taiwan, Republic of China
E-mail: tjhuang@che.nthu.edu.tw

$Y_{0.6}Sr_{0.4}Mn_{1-y}Co_yO_3$ ($0 \leq y \leq 0.4$) perovskite oxides were prepared by the coprecipitation method. The effect of Co substitution for Mn on the crystal structure, electrical conductivity and thermal expansion properties were investigated. By X-ray powder diffraction, the crystal structure was found to change from hexagonal symmetry of $Y_{0.8}Sr_{0.2}MnO_3$ to orthorhombic of $Y_{0.6}Sr_{0.4}Mn_{1-y}Co_yO_3$. The differences in the structure of the unsubstituted $Y_{1-x}Sr_xMnO_3$ ($0.2 \leq x \leq 0.4$) are attributed to the average ionic radii of the cations and the amounts of Mn^{4+} present. The results of electrical conductivity analysis can be described by the small polaron hopping conductivity model. With Co substitution, the activation energy increases, possibly due to an increase of Jahn–Teller distortion, at an extent higher than the increase of the concentration of charge carriers; thus, the electrical conductivity decreases. In addition, the relative densities of the materials reached ~94% with sintering at 1350°C for 12 h and had higher concentration of the available lattice sites, thus showing higher conductivity, than that with sintering at 1300°C for 6 h, which achieved ~70% relative density. It is also found that the thermal expansion coefficient (TEC) increases as the Sr and Co content of $Y_{1-x}Sr_xMn_{1-y}Co_yO_3$ increases and those with Co content of $y = 0.2$ exhibit TEC compatibility with YSZ.

Nomenclature

a	Lattice spacing
A	Pre-exponential factor
C	Fraction of available lattice sites occupied by charge carriers
d	Sintered density (g/cm^3)
d_{th}	Theoretical XRD density (g/cm^3)
d/d_{th}	Relative density (%)
e	unit charge (1.6×10^{-19})
E_a	Hopping activation energy (eV)
E_g	Energy gap (eV)
k	Boltzmann constant (8.63×10^{-5} eV/k)
n	Concentration of charge carriers (1/cm^3)
N	Concentration per formula unit of lattice sites (site/cm^3)
T	Absolute temperature (k)
α	Thermal expansion coefficient (1/°C)
σ	Electrical conductivity (S/cm)
μ	Mobility of charge carriers (cm^2/V · sec)
ν	Vibrational frequency (1/sec)

1. Introduction

The ideal cathode material of a solid oxide fuel cell (SOFC) should have high values of both electrical and oxygen-ion conductivities, high catalytic activity for oxygen molecule reduction, chemical stability with regard to yttria-stabilized zirconia (YSZ) electrolyte and interconnection material, and well-matched thermal expansion coefficient (TEC) with other cell components [1]. Currently, an Sr-doped $LaMnO_3$ perovskite oxide is used as the cathode material for SOFC because of its high electrical conductivity. However, its oxygen-ion conductivity is low [2], its thermal expansion coefficient is higher than that of YSZ, and it forms phases of $La_2Zr_3O_7$ and Sr_2ZrO_4, with low conductivities, at the interface with YSZ [3, 4]. A logical approach to this problem would be to simply replace La^{3+} in $La_{0.8}Sr_{0.2}MnO_3$ (LSM) with Y^{3+}, e.g., the $Y_{0.8}Sr_{0.2}MnO_3$ system. But, the latter has lower conductivity than that of LSM and lower thermal expansion coefficient than that of YSZ [5, 6].

The electrical conductivity of cobaltite perovskite oxide is known to be much higher than that of $La_{1-x}Sr_xMnO_3$ [7] and its polarization losses should be low due also to high oxygen-ion conductivity. The high values of both electrical and oxygen-ion conductivities for cathode materials lead to a substantial improvement in their electrochemical properties. Unfortunately, this is usually accompanied by a large increase in the thermal expansion coefficient. Thus, partial substitution of Co for Mn in $Y_{1-x}Sr_xMnO_3$ brings about not only an increase in electrical conductivity but also good ionic conductivity. Besides, it will cause only a slight increase in thermal expansion coefficient. Nevertheless,

*Author to whom all correspondence should be addressed.

in the case of substitutionally mixed systems, the electrical conductivity may be influenced by the interaction between the two transition metals, and the occurrence of trapping of charge carriers has been reported [8]. Accordingly, studies of electrical conductivities and crystal structures of various compositions in this system should be performed. In addition, it is important to understand the mechanism of electrical conductivity of the electrode materials.

The aims of the present investigation are to study the effect of Co substitution for Mn on the crystal structure, the electrical conductivity, and the thermal characterization of $Y_{0.6}Sr_{0.4}Mn_{1-y}Co_yO_3$ $(0 \leq y \leq 0.4)$ and to compare its properties with those of $Y_{0.8}Sr_{0.2}MnO_3$.

2. Experiment details

$Y_{1-x}Sr_xMn_{1-y}Co_yO_3$ powders were prepared by the coprecipitation method. Starting materials of $Y(CH_3COO)_3$, $Sr(CH_3COO)_2$, $Mn(CH_3COO)_2 \cdot 4H_2O$ and $Co(CH_3COO)_2 \cdot 4H_2O$ were dissolved in distilled water, in correct molar proportions. The precipitate/gel was formed when the acetate solution was dropped into the excessive NH_4OH solution, then the precipitate/gel solution was mixed with excess 1-octanol. The final solution was evaporated on a hot plate until the powder was obtained. After the organic compounds were burnt out at 600°C for 2 h, the powders were calcined in air at 1100°C for 5 h.

The crystal structure and lattice parameters of the synthesized powders were determined at room temperature by X-ray powder diffraction (XRD). The measurements were performed in the range of 20° to 80° 2θ at a scan rate of 4° 2θ/min with Cu K_α radiation.

The powders were compacted in the shape of disc (approximately 15 mm diameter by 1.6 mm thick) and then sintered in air at 1300°C for 6 h and at 1350°C for 12 h, respectively. The microstructure was analyzed with Scanning Electron Microscopy (SEM, JEOL JSM-5600) and the bulk density of the sintered sample was determined by the Archimedes method using distilled water.

The electrical conductivity was measured as a function of temperature on the sintered disc specimens by the four-probe method on direct current. Platinum wires (0.3 mm thick) were used as current and potential leads and the measurements were carried out in the temperature range of 500–950°C in increments of 50°C. Measurement of the thermal expansion coefficient was performed in air at a cooling rate of 5°C/min from 900°C to room temperature.

3. Results and discussion

3.1. Crystal structure

X-ray powder diffraction (XRD) was performed on the synthesized powders to determine the phases. Fig. 1 shows the XRD patterns of $Y_{1-x}Sr_xMn_{1-y}Co_yO_3$ materials with sintering at 1300°C for 6 h. As seen in Fig. 1, $Y_{1-x}Sr_xMn_{1-y}Co_yO_3$ appears to exist in both hexagonal non-perovskite and orthorhombic perovskite phases. For Sr content $(x) = 0.2$ to 0.4, there is a change in the structure and symmetry of the $Y_{1-x}Sr_xMnO_3$ materials from non-perovskite hexagonal $P6_3$ cm to perovskite orthorhombic Pbnm.

The lack of stability of the perovskite form of $Y_{0.8}Sr_{0.2}MnO_3$ can be attributed to that the average ionic radii of the Y^{3+} and Sr^{2+} cations (Table I) are too small to act as the A site cations, such as for $YMnO_3$,

TABLE I Ionic radii of several cations in $Y_{1-x}Sr_xMn_{1-y}Co_yO_3$ perovskite lattices [12]

Cation	Ionic radius (Å)
Y^{3+}	1.18
Sr^{2+}	1.44
Mn^{3+}	0.645
Mn^{4+}	0.530
Co^{3+}	0.545
Co^{4+}	0.530

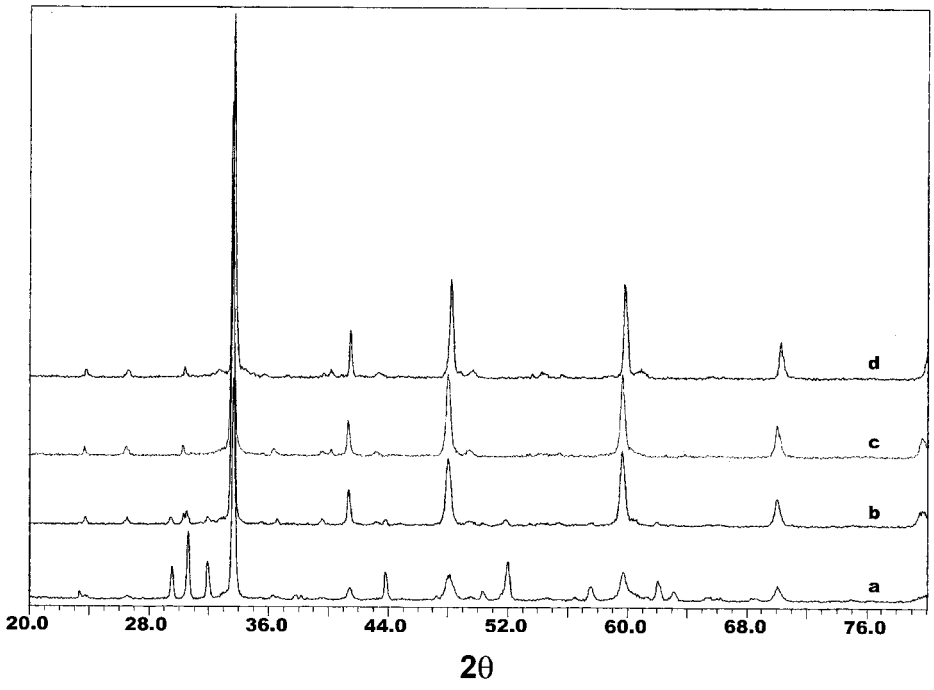

Figure 1 XRD patterns of $Y_{1-x}Sr_xMn_{1-y}Co_yO_3$ materials. *a*: $x = 0.2$, $y = 0.0$; *b*: $x = 0.4$, $y = 0.0$; *c*: $x = 0.4$, $y = 0.2$; *d*: $x = 0.4$, $y = 0.4$.

TABLE II Phase symmetry, lattice parameters, and unit cell volume of $Y_{1-x}Sr_xMn_{1-y}Co_yO_3$ perovskite system at room temperature

Composition	Phase symmetry	a (Å)	b (Å)	c (Å)	Volume (Å^3)	$c/\sqrt{2}$ (Å)	$a, b, c/\sqrt{2}$ relation
$x=0.2$, $y=0.0$	Hexagonal	6.076		11.44	422.34		
$x=0.4$, $y=0.0$	Orthorhombic	5.4735	5.6676	7.3221	227.12	5.1775	$c/\sqrt{2}<a<b$
$x=0.4$, $y=0.2$	Orthorhombic	5.4630	5.6460	7.3194	225.76	5.1756	$c/\sqrt{2}<a<b$
$x=0.4$, $y=0.4$	Orthorhombic	5.4604	5.6359	7.3162	225.15	5.1733	$c/\sqrt{2}<a<b$

TABLE III Measured sintered densities at two different sintering conditions (d_1 and d_2), theoretical XRD density (d_{th}), and relative density (d/d_{th}) of $Y_{0.6}Sr_{0.4}Mn_{1-y}Co_yO_3$

Composition	Sintered density at 1300°C for 6 h d_1 (g/cm^3)	Sintered density at 1350°C for 12 h d_2 (g/cm^3)	XRD density d_{th} (g/cm^3)	Relative density at 1300°C for 6 h d_1/d_{th} (%)	Relative density at 1350°C for 12 h d_2/d_{th} (%)
$y=0$	4.354	5.346	5.5930	78	96
$y=0.2$	4.059	5.289	5.6503	72	94
$y=0.4$	4.33	5.334	5.6892	76	94

which has two polymorphs [9]. Under high pressure or high temperature condition, $YMnO_3$ is an orthorhombic perovskite, but generally it crystallizes to a hexagonal non-perovskite structure [9–11]. The mechanism of structure transition with Sr substitution for Y in yttrium manganite is due chiefly to the steric effect, i.e., the change in the average ionic radius and the decrease in the lattice distortion. In fact, the presence of Mn^{4+} favors the stabilization of the perovskite phase and decreases the degree of MnO_6 octahedra distortion [10]; phase transformation occurs with varying Mn^{4+} content in yttrium manganites, e.g., when substituting divalent ions in yttrium site. Thus, as has been indicated above, $Y_{1-x}Sr_xMnO_3$ shows a change of crystalline structure when the Sr content increases.

For $Y_{0.6}Sr_{0.4}Mn_{1-y}Co_yO_3$ $(0 \le y \le 0.4)$, the patterns have been indexed as orthorhombic structure [10]. The calculated lattice parameters are shown in Table II. Each unit cell consists of four ABO_3 units, and the parameters are related to a_0 as $a=\sqrt{2}a_0$, $b=\sqrt{2}a_0$, $c=2a_0$, where $a_0=4$ Å for ideal cubic perovskite. On substitution of Mn by Co, the structure does not undergo any change but there is a systematic decrease in the lattice parameter as the Co content increases. The decrease in the lattice constant can be related to smaller ionic radius of the Co ion. For a fixed composition at the A-site of $Y_{0.6}Sr_{0.4}Mn_{1-y}Co_yO_3$, inspection of the transition metal ionic radii (Table I) reveals that, while the tetravalent Co and Mn ions have equal sizes, the Co^{3+} cation is smaller than the M^{3+} cation. Therefore, the unit cell volume also decreases with increasing Co content.

The relation among the lattice parameters, a, b and $c/\sqrt{2}$, can provide a measure of the distortion of the unit cell. This relation is also shown in Table II. It is seen that $c/\sqrt{2}<a<b$ in all cases. This is characteristic of the O′-type orthorhombic and is originated by the strong cooperative Jahn–Teller effect, which induces an orbital ordering and distorts the BO_6 octahedra. This is in contrast with the usual situation in perovskites where the primary distortion effect is steric and $c/\sqrt{2}$ lies between a and b.

3.2. Sintering and microstructure

In Table III, the measured sintered density (d), the theoretical XRD density (d_{th}), and the relative density (d/d_{th}) are given. The sintered density of $Y_{0.6}Sr_{0.4}Mn_{1-y}Co_yO_3$ after sintering at 1300°C for 6 h was about 70% of the theoretical density. Since several of the bulk properties are related to the sintered density and the microstructure of the materials [13], dense sample must be obtained in order to measure the thermal expansion coefficient and the electrical conductivity of the ceramic materials. An acceptable relative density of the ceramic sample for measuring the mechanical properties is ≥90%. In general, the sintered density of the ceramics depends on the sintering temperature as well as the holding time; thus, relative densities greater than 94% were attained after sintering at 1350°C for 12 h.

The microstructures developed by the sintered bodies at two different sintering conditions are shown in Figs 2 and 3, respectively. The grain shape is irregular and the size distribution is heterogeneous. Inter-granular voids can be seen. Compared the SEM images of Figs 2 and 3, it is seen that the material with lower density has larger voids than that of higher density. This result is expected to occur due to grain growth and secondary crystallization [14]. When grain growth occurs, many voids become isolated from grain boundaries. In the presence of voids, the boundaries are able to move and the grains with highly curved boundaries are able to grow. With increasing sintering temperature and time, the process of secondary crystallization may occur when a fraction of the grains grow to a larger size. For these reasons, grain growth appears perfectly straight on the boundaries and some larger grains can be achieved after sintering at 1350°C for 12 h. Thus, material with higher sintered density has larger grains.

It is also worthy to note that the materials of $Y_{0.8}Sr_{0.2}MnO_3$ (i.e., $x=0.2$ and $y=0.0$) sintered at both sintering conditions show microcracks. The microcracking seems to be caused by a high-temperature phase transition between hexagonal and orthorhombic of $Y_{0.8}Sr_{0.2}MnO_3$ [5].

3.3. Electrical conductivity

Electrical conductivities of $Y_{1-x}Sr_xMn_{1-y}Co_yO_3$ after sintering at the above-mentioned two conditions (i.e., 1300°C for 6 h and 1350°C for 12 h) are shown in Figs 4 and 5, respectively. The conductivity increases with increasing sintering temperature but decreases as the

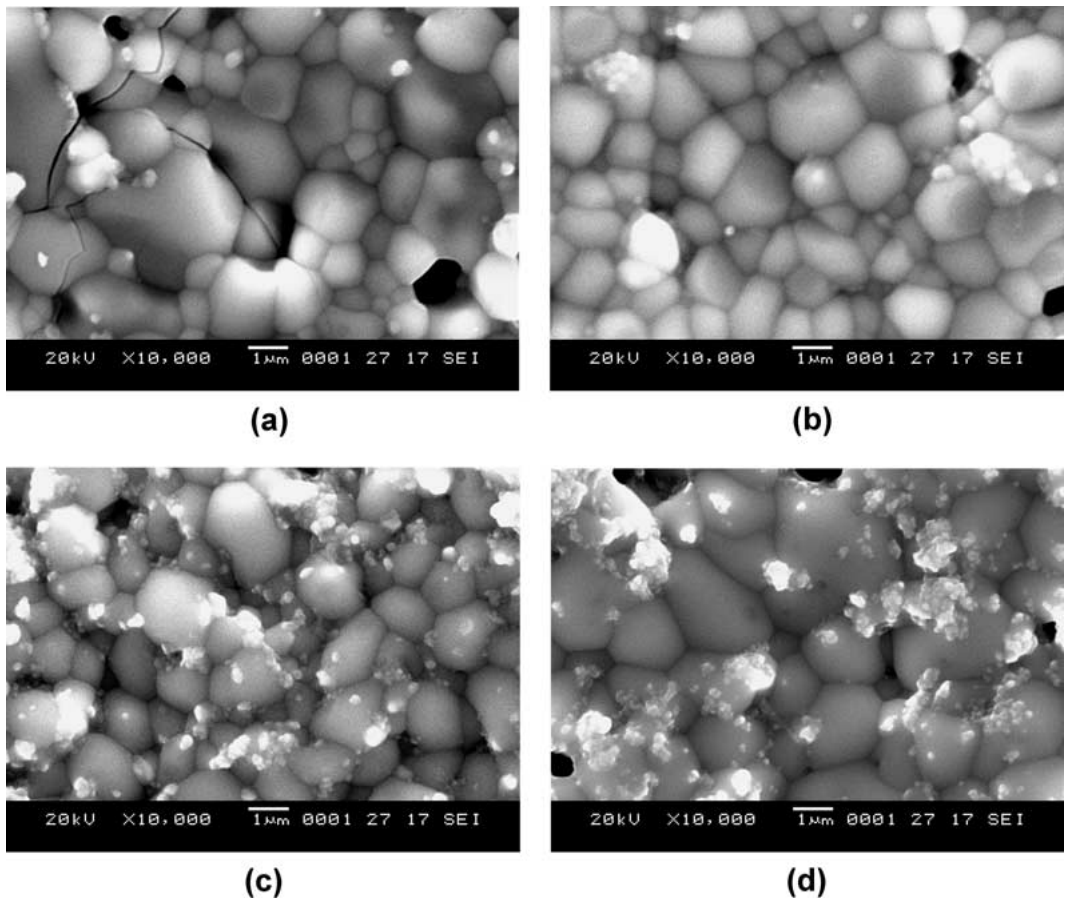

Figure 2 SEM micrographs of $Y_{1-x}Sr_xMn_{1-y}Co_yO_3$ samples: (a) $x = 0.2$, $y = 0.0$; (b) $x = 0.4$, $y = 0.0$; (c) $x = 0.4$, $y = 0.2$; (d) $x = 0.4$, $y = 0.4$. These samples were sintered at 1300°C for 6 h.

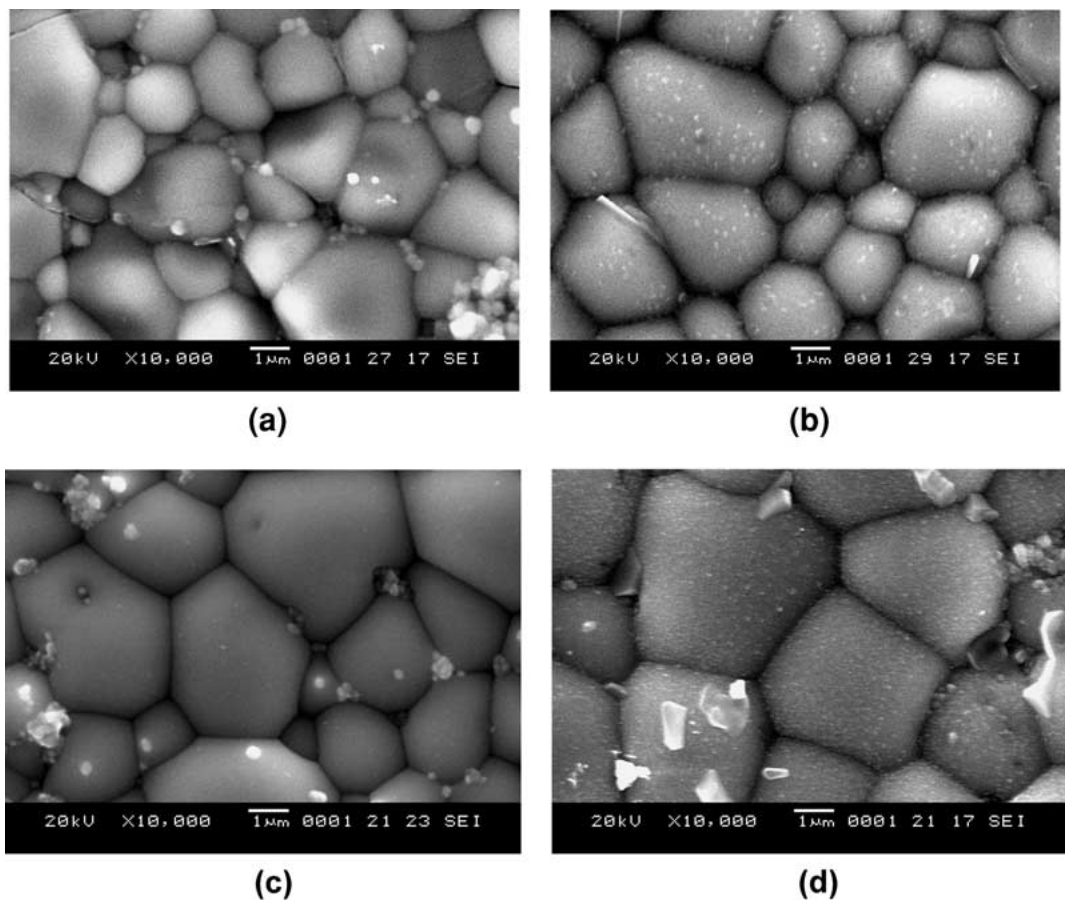

Figure 3 SEM micrographs of $Y_{1-x}Sr_xMn_{1-y}Co_yO_3$ samples: (a) $x = 0.2$, $y = 0.0$; (b) $x = 0.4$, $y = 0.0$; (c) $x = 0.4$, $y = 0.2$; (d) $x = 0.4$, $y = 0.4$. These samples were sintered at 1350°C for 12 h.

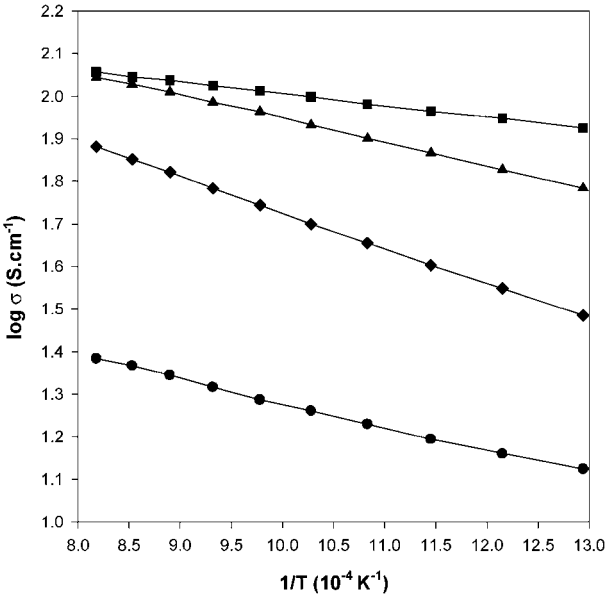

Figure 4 log (σ) vs. $1/T$ for $Y_{1-x}Sr_xMn_{1-y}Co_yO_3$ sintered at 1300°C for 6 h. ●: $x = 0.2$, $y = 0.0$; ■: $x = 0.4$, $y = 0.0$; ▲: $x = 0.4$, $y = 0.2$; ♦: $x = 0.4$, $y = 0.4$.

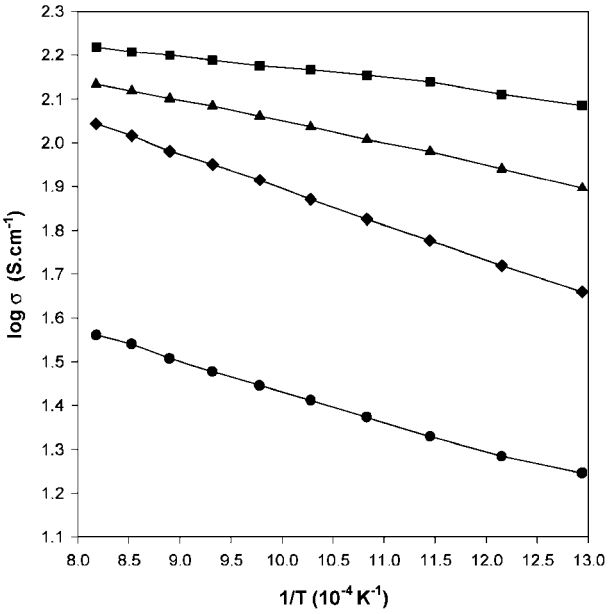

Figure 5 log (σ) vs. $1/T$ for $Y_{1-x}Sr_xMn_{1-y}Co_yO_3$ sintered at 1350°C for 12 h. ●: $x = 0.2$, $y = 0.0$; ■: $x = 0.4$, $y = 0.0$; ▲: $x = 0.4$, $y = 0.2$; ♦: $x = 0.4$, $y = 0.4$.

Co content (i.e., the y value) increases for orthorhombic $Y_{0.6}Sr_{0.4}Mn_{1-y}Co_yO_3$ ($0 \leq y \leq 0.4$). The temperature dependence of the electrical conductivity of the oxides of this study indicates a semi-conducting behavior, which can be described by the small polaron hopping conductivity model. Generally, the electrical conductivity, σ, is expressed as

$$\sigma = ne\mu \tag{1}$$

where e is the unit charge and n is the concentration of charge carriers. n is given as

$$n = N\exp(-E_g/2kT) = NC \tag{2}$$

where E_g is the energy required to create cations of different charges by separating an excited electron from the hole it leaves behind [15], N is the concentration per formula unit of lattice sites which are available to the charge carriers, and C is a fraction of the available lattice sites occupied by the charge carriers.

The mobility of charge carriers, μ, is given as

$$\mu = [(1 - C)ea^2\nu/kT]\exp(-E_a/kT) \tag{3}$$

where a and ν are the lattice spacing and vibrational frequency, respectively. k is the Boltzmann constant, T is absolute temperature, and E_a is a hopping activation energy [16].

The temperature dependence of conductivity is described in the expressions of n and μ. For oxide semiconductors, n and μ usually increase with temperature. Hence, conductivity increases with temperature. Nevertheless, at equilibrium condition and in air, the concentration of electron holes (charge carriers) is maintained to be constant. Therefore, Equation 2 can be rewritten as

$$n = NC = \text{constant}$$

and thus the temperature dependence of conductivity is described only by μ, as in Equation 3. With Equation 3 being substituted in Equation 1, the expression for the temperature-dependent electrical conductivity of the small polaron material becomes

$$\sigma = (A/T)\exp(-E_a/kT) \tag{4}$$

where A is the pre-exponential factor, defined as

$$A = NC(1 - C)e^2a^2\nu/k \tag{5}$$

With Equation 4, the plots of log (σT) vs. $1/T$ for $Y_{1-x}Sr_xMn_{1-y}Co_yO_3$ with the two sintering conditions are illustrated in Figs 6 and 7, respectively. It can be seen that these plots are straight lines for all compositions. According to these results, it may be stated that the conductivity mechanism is by thermally activated hopping of small polarons between localized states corresponding to Mn and Co sites of different valence value. The slopes of these straight lines were

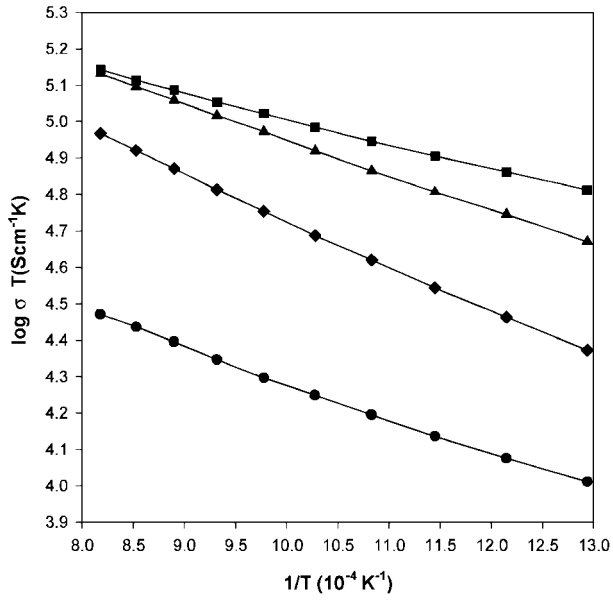

Figure 6 log (σT) vs. $1/T$ for $Y_{1-x}Sr_xMn_{1-y}Co_yO_3$ sintered at 1300°C for 6 h. ●: $x = 0.2$, $y = 0.0$; ■: $x = 0.4$, $y = 0.0$; ▲: $x = 0.4$, $y = 0.2$; ♦: $x = 0.4$, $y = 0.4$.

TABLE IV Pre-exponential factor (A), hopping activation energy (E_a), and electrical conductivity (σ) of $Y_{1-x}Sr_xMn_{1-y}Co_yO_3$

Composition	Sintered at 1300°C for 6 h			Sintered at 1350°C for 12 h		
	A_1 (10^5)	E_{a1} (eV)	σ800°C,1	A_2 (10^5)	E_{a2} (eV)	σ800°C,2
$x=0.2$, $y=0.0$	1.83	0.194	20.76	3.44	0.218	30.02
$x=0.4$, $y=0.0$	5.07	0.138	105.72	7.32	0.137	153.62
$x=0.4$, $y=0.2$	8.37	0.193	96.91	9.67	0.188	119.53
$x=0.4$, $y=0.4$	9.74	0.250	60.81	13.45	0.244	89.81

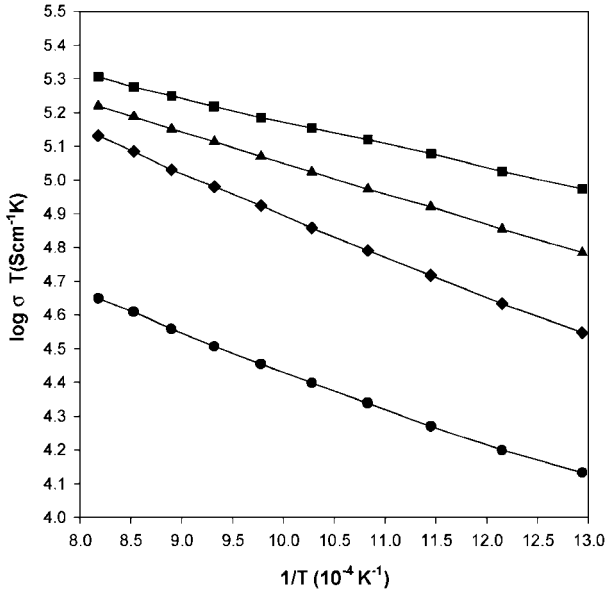

Figure 7 $\log(\sigma T)$ vs. $1/T$ for $Y_{1-x}Sr_xMn_{1-y}Co_yO_3$ sintered at 1350°C for 12 h. ●: $x=0.2$, $y=0.0$; ■: $x=0.4$, $y=0.0$; ▲: $x=0.4$, $y=0.2$; ♦: $x=0.4$, $y=0.4$.

applied to obtain the activation energy, E_a, and to evaluate the pre-exponential factor, A. The electrical conductivity, activation energy and pre-exponential factor for $Y_{1-x}Sr_xMn_{1-y}Co_yO_3$ are summarized in Table IV.

For the unsubstituted $Y_{1-x}Sr_xMnO_3$ ($0.2 \le x \le 0.4$) with the same sintering condition, the material of $x=0.4$ with perovskite structure has higher conductivity but lower activation energy for conductivity than that of $x=0.2$. It has been reported that the substitution of trivalent lanthanide ions by divalent alkaline earth ions leads to the simultaneous occurrence of Mn^{3+} and Mn^{4+} ions in the B-position of the crystal lattice, and this significantly modifies the structure and electrical properties [17]. The conductivity dependence of $Y_{1-x}Sr_xMnO_3$ on the strontium ion content is well correlated with the dependence of the Mn^{4+} ion concentration on the content of the doping additive. Further, the structure is orthorhombic for high Sr^{2+} content of $Y_{0.6}Sr_{0.4}MnO_3$ and the charge carriers are transported by the Mn^{3+}–O–Mn^{4+} network. The above-mentioned microcracking in $Y_{0.8}Sr_{0.2}MnO_3$ is also expected to preclude the transfer of charge carriers. It is thus reasonable to expect that the hopping activation energy (E_a) of orthorhombic $Y_{0.6}Sr_{0.4}MnO_3$ is lower than that of hexagonal $Y_{0.8}Sr_{0.2}MnO_3$, and the former material shows a higher conductivity.

For Co-substituted $Y_{0.6}Sr_{0.4}MnO_3$ with orthorhombic structure, the activation energy increases with increasing Co content. This can be described by the concept of small polarons, which can arise from the strong lattice–electron interaction originating from the Jahn–Teller distortion [18]. It is well known that the substitution of divalent ions for La in $LaMnO_3$, and hence the formation of tetravalent Mn ions, removes the lattice distortion; since the Y system is expected to show similar behavior with the La system, it is assumed in this work that $YMnO_3$ would show similar behavior with $LaMnO_3$ in this aspect. Thus, when Co is substituted for the Mn ions, the amount of Mn^{4+} in the system decreases, according to the reaction of

$$Co^{2+} + Mn^{4+} = Co^{3+} + Mn^{3+} \qquad (6)$$

and it is likely that a certain amount of lattice distortion arises again. Since the amount of Mn^{4+} decreases with increasing Co substitution, the strong carrier localization in the mixed system most likely has its origin in the lattices distortion and the resulting polaron formation. A distortion of B—O—B bond narrows energy band width and thus reduces the charge carrier transfer between two metal sites. Consequently, lattice distortion increases the activation energy for charge carrier hopping [19].

Theoretically, the conductivity of $Y_{1-x}Sr_xMn_{1-y}Co_yO_3$ in air is related to both the mobility and the concentration of charge carriers (electron holes). In addition, the transfer rate (mobility) of charge carriers can be determined by the hopping activation energy due to the Jahn–Teller distortion. And, the concentration of charge carriers can be related to the pre-exponential factor, A, which has been related to the concentration of the available lattice sites (N) and fraction of available sites occupied (C), as shown in Equation 5. Also noted that C is related to the energy gap (E_g), as seen in Equation 2. Therefore, given localized d electrons, an increase in the Co-ion population leads to a decrease in E_g; this means that the onset and increase of short-range order should be accompanied by an abrupt increase in the slope of electrical conductivity vs. temperature [20].

The concentration of the available lattice sites can be expected to depend on the grains formed in response to the sintering condition. The SEM and d/d_{th} results of $Y_{0.6}Sr_{0.4}Mn_{1-y}Co_yO_3$ with fixed sintering temperature and holding time show that the sizes and quantities of the grains are similar. It is suggested that the concentration of the available lattice sites is the same for all three compositions of y. Hence, the increase in the concentration of charge carriers is attributed to the decrease of energy gap (E_g) due to Co substitution. However, the effect of the increase of Jahn–Teller distortion is larger than that of the decrease of energy gap. This means that the transfer rate of charge carriers decreases with

TABLE V Thermal expansion coefficient of $Y_{1-x}Sr_xMn_{1-y}Co_yO_3$

Composition	$\alpha(10^{-6}/°C)$	Reference
$x=0.2$, $y=0.0$	6.78	This work
$x=0.4$, $y=0.0$	8.28	This work
$x=0.4$, $y=0.2$	9.86	This work
$x=0.4$, $y=0.4$	12.2	This work
YSZ	10.3	[3]

increasing Co substitution. Therefore, the conductivity of $Y_{0.6}Sr_{0.4}Mn_{1-y}Co_yO_3$ decreases with increasing Co content, as shown in Table IV.

On the other hand, for the same composition, the conductivity of the material sintered at 1350°C for 12 h is higher than that sintered at 1300°C for 6 h. Based on the results of Table IV, the measured hopping activation energies at different sintering conditions are similar for same Co content in $Y_{0.6}Sr_{0.4}Mn_{1-y}Co_yO_3$, which has same energy gap. Since the electrical conductivity is known to depend on the microstructure and density [13], the increase in conductivity may be due to the increase of sintered density. In other words, the size of the grains and the concentration of the available lattice sites increase with increasing sintering temperature and time for sintered bodies. The better contacts between the grains and the interconnected voids in the sintered bodies with higher sintering temperature and longer time (Fig. 3) may also be responsible for the higher conductivity observed.

3.4. Thermal expansion

Table V shows the thermal expansion coefficient (TEC) of $Y_{1-x}Sr_xMn_{1-y}Co_yO_3$ in air. It is seen that TEC increases with increasing Sr and Co content. This may be explained with electron hopping.

At a higher temperature, the electrical conductivity becomes higher, as observed above; thus, with a larger concentration of Co, the mobile electrons may be easier to hop from Co^{2+} to Mn^{4+} according to the reaction of Equation 6 and thus the B-site ions, i.e., the Mn ions, are easier to be reduced from higher to lower valence state ($Mn^{4+} \rightarrow Mn^{3+}$). Considering the larger size of Mn^{3+} cation with respect to Mn^{4+}, as shown in Table I, it is apparent that the unit cell volume increases. Therefore, the extent of thermal expansion increases.

In addition, it is seen that the $Y_{1-x}Sr_xMn_{1-y}Co_yO_3$ material with $x=0.4$ and $y=0.2$ exhibits TEC compatibility with YSZ and thus would best suit application with the YSZ electrolyte.

4. Conclusion

It was confirmed that the unsubstituted $Y_{1-x}Sr_xMnO_3$ ($0.2 \leq x \leq 0.4$) has a structure transition from hexagonal ($x=0.2$) to O′-orthorhombic phase ($x=0.4$). Increasing sintering temperature and holding time conduce to grain growth and secondary crystallization, so that the relative density of $Y_{0.6}Sr_{0.4}Mn_{1-y}Co_yO_3$ reached 94% after sintering at 1350°C for 12 h and the electrical conductivity for the material with a fixed Co content increases.

The structure of $Y_{0.8}Sr_{0.2}MnO_3$ is a hexagonal phase and the microcracking may exist and be obstacle in the charge carrier transfer, thereby decreasing the electrical conductivity. The B-site substitutionally-mixed systems are not expected to enhance the electrical conductivities of $Y_{0.6}Sr_{0.4}Mn_{1-y}Co_yO_3$.

The substitution of Co for Mn in $Y_{0.6}Sr_{0.4}MnO_3$ leads to the increase of both the Jahn–Teller distortion and the concentration of charge carriers. The increase of the Jahn–Teller distortion increases the hopping activation energy (E_a); this decreases the electrical conductivity. In addition, the effect of Co substitution on the increase of the activation energy is higher than that on the increase of the concentration of charge carriers. Thus, the electrical conductivity decreases with increasing Co content in $Y_{0.6}Sr_{0.4}Mn_{1-y}Co_yO_3$ with orthorhombic structure.

In addition, it was observed that the thermal expansion coefficient of the material increases with increasing Sr and Co content. This may be explained with electron hopping.

References

1. P. J. GELLINGS and H. J. M. BOUWMEESTER, in "The CRC Handbook of Solid State Electrochemistry" (CRC Press, New York, 1997) p. 407.
2. J. H. KUO, H. U. ANDERSON and D. M. SPARLIN, *J. Solid State Chem.* **87** (1990) 55.
3. H. U. ANDERSON, *Solid State Ionics* **52** (1992) 33.
4. O. YAMAMOTO, Y. TAKEDA, R. KANNO and M. NODA, *ibid.* **22** (1987) 241.
5. B. FU and W. HUEBNER, *Mater. Res. Soc.* **9** (1994) 2645.
6. L. A. TIKHONOVA, P. P. ZHUK, A. A. VECHER and M. V. ZINKEVICH, *Inorg. Mater.* **28** (1992) 1535.
7. N. GUNASEKARAN, N. BAKSHI, C. B. ALCOCK and J. J. CARBERRY, *Solid State Ionics* **83** (1996) 145.
8. R. RAFFAELLE, H. U. ANDERSON, D. M. SPARLIN and P. E. PARRIS, *Phys. Rev. Lett.* **65** (1990) 1383.
9. J. W. STEVENSON, M. M. NASRALLAH, H. U. ANDERSON and D. M. SPARLIN, *J. Solid State Chem.* **102** (1993) 175.
10. J. A. ALONSO and M. J. MARTÍNEZ-LOPE, *Inorg. Chem.* **39** (2000) 917.
11. C. MOURE, M. VILLEGAS, J. F. FERNANDEZ, J. TARTAJ and P. DURAN, *J. Mater. Sci.* **34** (1999) 2565.
12. R. D. SHANNON, *Acta Crtallogr. A* **32** (1976) 751.
13. M. KERTESZ, I. RIESS, D. S. TANNHAUSER, R. LANGPAGE and F. J. ROHR, *J. Solid State Chem.* **42** (1982) 125.
14. M. H. HUANG, Ph. D Thesis, Imperial College, London (1991) p. 118.
15. J. B. GOODENOUGH, *J. Appl. Phys.* **37** (1966) 1415.
16. R. KOC and H. U. ANDERSON, *J. Eur. Ceram. Soc.* **15** (1995) 867.
17. E. POLLERT, S. KRUPICKA and E. KUZMICOVA, *J. Phys. Chem. Solid* **43** (1982) 1137.
18. N. GAYATHRI, A. K. RAYCHAUDHURI and S. K. TIWARY, *Phys. Rev. B* **56** (1997) 1345.
19. S. Y. BAE, D. J. SNYDER and S. X. WANG, *J. Electr. Mater.* **27** (1998) 1.
20. P. M. RACCAH and J. B. GOODENOUGH, *Phys. Rev.* **155** (1967) 932.

Received 19 November 2001
and accepted 3 July 2002